Travelling waves and spatial hierarchies in measles epidemics

B. T. Grenfell*, O. N. Bjørnstad*† & J. Kappey*

* *Zoology Department, University of Cambridge, Downing Street, Cambridge CB2 3EJ, UK*
† *501 ASI Building, Departments of Entomology and Biology, Penn State University, University Park, Pennsylvania 16802, USA*

Spatio-temporal travelling waves are striking manifestations of predator–prey and host–parasite dynamics. However, few systems are well enough documented both to detect repeated waves and to explain their interaction with spatio-temporal variations in population structure and demography. Here, we demonstrate recurrent epidemic travelling waves in an exhaustive spatio-temporal data set for measles in England and Wales. We use wavelet phase analysis, which allows for dynamical non-stationarity—a complication in interpreting spatio-temporal patterns in these and many other ecological time series. In the pre-vaccination era, conspicuous hierarchical waves of infection moved regionally from large cities to small towns; the introduction of measles vaccination restricted but did not eliminate this hierarchical contagion. A mechanistic stochastic model suggests a dynamical explanation for the waves—spread via infective 'sparks' from large 'core' cities to smaller 'satellite' towns. Thus, the spatial hierarchy of host population structure is a prerequisite for these infection waves.

Travelling waves, arising essentially from activator–inhibitor dynamics[1–3], are predicted by theory in a range of host–natural enemy systems[1,4–8]. However, except as the product of invasion dynamics[9], empirical observations of waves are comparatively rare—especially repeated periodic waves associated with host–natural enemy population cycles[7,8,10–12]. Even where waves are dynamically possible, they may not be detected because of a lack of spatio-temporal data at the appropriate resolution. More subtly, spatial heterogeneities in population density or demography[8,13] and temporal changes in parameters (resulting, for example, from vaccination against disease[1,6]), can significantly alter the detection and dynamics of spatio-temporal waves. The integration of models and data to explore these interactions between spatial dynamics and host demography is often prevented by a lack of demographic information.

Childhood microparasitic infections—in particular, historical measles epidemics in developed countries—provide sufficiently detailed spatio-temporal data on disease incidence and host demography[14,15] to address these issues. The task is aided by epidemiological models[16–21], which capture both the nonlinear dynamics of childhood epidemics as a function of local population size[16] and the impact of significant environmental forcing. This forcing mainly comprises seasonality in transmission, due to schooling patterns[17], and longer-term variations in susceptible recruitment, due to birth-rate variations and the onset of vaccination[20,22]. Such long-term temporal changes in dynamic rates give rise to non-stationarity in the resulting ecological time series.

The detection of temporal and spatio-temporal oscillations in time series is greatly complicated by non-stationary temporal variations in dynamical behaviour (such as changes in mean, variance, period of oscillations, and so on). In particular, trends or sudden jumps in cycle period complicate the search for temporal and spatial patterns, since conventional frequency-domain analyses assume stationarity[23,24]. Figure 1a illustrates the periodic but non-stationary dynamics of weekly measles notifications for London for the period 1944–94. There are marked changes in epidemic period between the 1940s and 1950s, as well as into the vaccine era (after 1968).

We apply wavelet time series analysis[23–26] to describe the non-stationarity in the period of recurrent epidemics of measles in England and Wales. Wavelet phase angles also reveal rapid spatio-temporal waves of infection, originating from regional centres. Finally we use a refined epidemiological model to suggest how such waves can arise in seasonal environments, and explore the role of spatial heterogeneities in creating them.

Local measles dynamics

Measles epidemics in developed countries generally exhibit seasonal cycles and longer-term (generally biennial) major epidemics[18,19,27]. However, the relative importance of the seasonal versus multiannual cycles varies with time. These features of the dynamics are clearly seen from a wavelet spectral analysis of the time series of weekly measles notifications for London from 1944 to 1994 (Box 1 and Fig. 1). The local wavelet power spectrum (Fig. 1b) shows the importance of the different oscillatory periods as a function of time. The seasonal cycles and (in general) biennial major epidemics are obvious, as also is the long-term non-stationarity in the period of the major epidemic. The main long-term change in dynamics accompanies the onset of vaccination in 1968 (Fig. 1b). After this, the annual periodicity is less marked and the intervening major epidemics (now of lower amplitude) gradually increase in period, compared to the pre-vaccine era. This gradual transition coincides with a steady increase in vaccine uptake from around 50% in the 1970s to around 90% in the late 80s (Fig. 1d). Theory predicts[18,20], and previous time-series analyses have confirmed[20,28], that vaccination should generate an increase in the epidemic period. Here we use the temporal dimension of the wavelet analysis to reveal the progressive nature of this increase (Fig. 1b).

To generate a synoptic picture of transitions in measles dynamics across 354 administrative areas of England and Wales (see Methods), we focus on changes through time in the dominant epidemic period (Fig. 1d). The regional pattern is remarkably consistent with the detailed analysis for London: biennial epidemics before widespread vaccination are followed by epidemics of longer period through the vaccine era. A second important feature of the pre-vaccination era is the reduction in inter-epidemic interval (to under 2 years) coinciding with the 1945–47 and 1962–65 'baby booms'[22]. All these transitions in disease dynamics are driven by 'extrinsic' variations in recruitment rate of susceptibles[20] (Fig. 1d) through changes in birth rates (discounted by vaccine uptake in the vaccination era). The analysis includes hundreds of locations, ranging from large cities (where there are regular epidemics) to small towns (where disease dynamics are strongly influenced by stochasticity[27]). Consequently, these results give an unusually

Box 1

Wavelet time series analysis

We introduce the basic principles of the method[23–26], as applied to measles in London. Traditional Fourier analysis partitions the total power (variance) of the time series between sinusoidal components at different frequencies[29]. If we apply this approach to series with a marked change in cycle period through time (such as Fig. 1a), the resulting spectrum reflects both scales of variation, but tells us nothing about their sequence. This is particularly problematic if the data show unusual 'spikes' and irruptions, or in the presence of smooth changes in periodicity[23].

By contrast, the essence of the wavelet approach is locality in time as well as frequency. Rather than a sinusoid, the method is based on a wavelet function, which can explore local variations in frequency. The last decade has seen an explosion of applications of wavelets in mathematics and its applications[25]; this has led to a wide range of wavelet functions.

In this paper, we use the Morlet wavelet function[23] (see Methods and Fig. 1e). The Morlet function is essentially a damped complex exponential, which can capture local (in time) cyclical fluctuations in the time series. As with all wavelets, the frequency–time range over which it does this is set by a scale parameter, s. In general, wavelet scale is related to the conventional Fourier period of oscillations (Methods).

A local wavelet power spectrum (LWPS; see Methods) of the weekly London measles time series (Fig. 1a) is presented in Fig. 1b–d. Power is colour-coded as shown. Seasonality in the epidemic generates a peak in power at approximately one year. The major peak in power varies around two years, as described in the text. The superimposed parabola is the cone of influence (see Methods), which measures the extent of edge effects. Only significant ($P < 0.05$) power is shown.

Time and scale averaging

A useful feature of the LWPS is that it can be averaged across both frequency and time (Methods[23]). Figure 1c shows the global wavelet spectrum, estimated by averaging the LWPS across time (the dotted line is the lower limit of significance). The global spectrum is analogous to the traditional Fourier spectrum. We note the annual and roughly biennial peaks of power. Other wavelet methods used here, such as the analysis of phase differences and smoothing by reconstruction of important frequencies, are discussed in the Methods.

As described in the text, Fig. 1d shows a synoptic summary across all spatial locations in England and Wales of the period of major epidemics (in the range 1.5–5 years). The blue line indicates the average of this period across 354 spatial locations in England and Wales; the thickness of the line represents ±1 standard error of the mean, s.e.m. The red line shows vaccination (p) rate. The black line is the effective recruitment rate of susceptibles, $B(1-p)$, where B is the birth rate (the relevant axis is suppressed: recruitment drops from a maximum of 0.021 per individual in 1947 to near zero by 1994). Figure 1d shows the progressive change from period 2 to period 3 dynamics over the 1970s and 80s. However, the subsequent increase to 4 years in the late 1980s and 90s should be interpreted cautiously, since it may reflect the secular decline at the end of the time series, caused by the major increase in vaccination uptake over this period.

Wavelet methods have considerable potential as tools for ecological time series and spatial analyses[38]. However, like many 'local' statistical methods, they need a lot of data—features can be detected only at a given time and frequency if the underlying process is sufficiently well sampled. It is also important to try a variety of wavelet functions[24]. A number of continuous and discrete functions can capture the basic patterns shown here; however, the Morlet function gives the clearest picture.

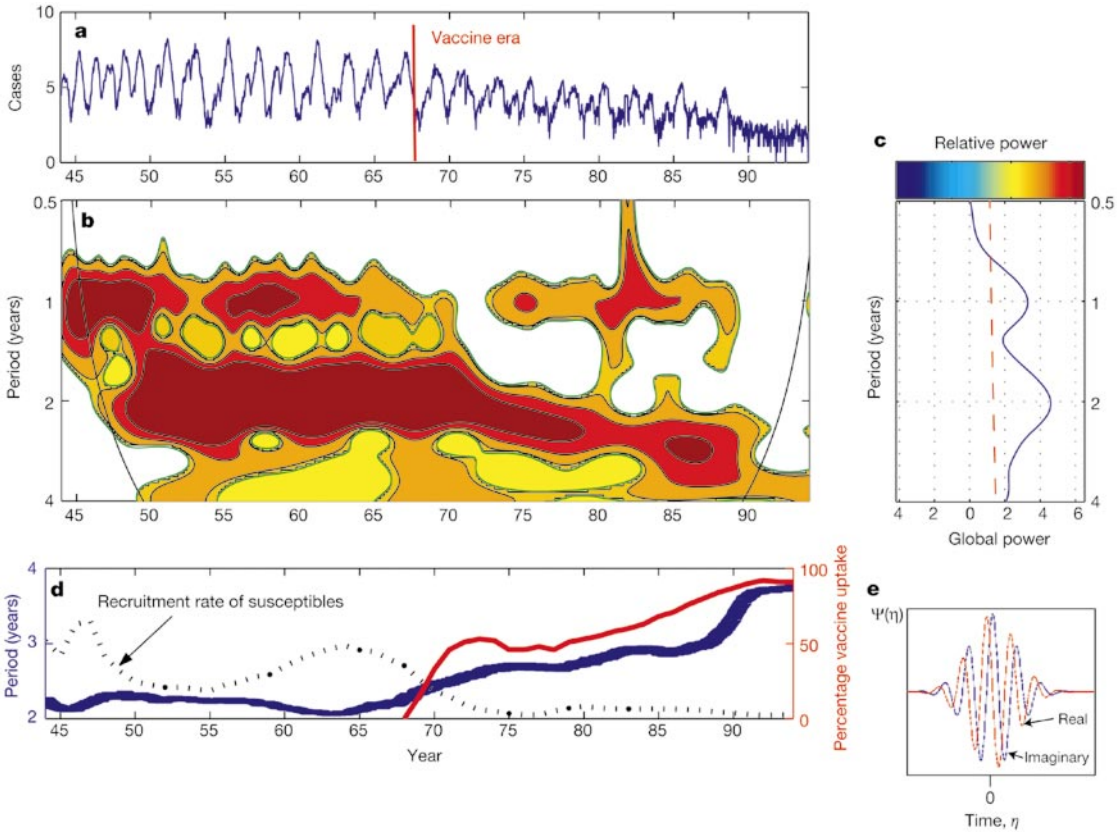

Figure 1 Wavelet time series analysis for the log-transformed weekly London measles time series (see Box 1 for details). **a**, The time series. **b**, Local wavelet power spectrum (LWPS); power is colour coded as shown on the key at top right. **c**, Global wavelet spectrum. **d**, Summary of temporal changes in the dominant epidemic period, averaged across towns and cities in England and Wales. **e**, Shape of the Morlet wavelet used in the analysis.

detailed picture of the influence of changes in host demography on epidemic dynamics.

Travelling waves and wavelet phase angles

We investigate spatio-temporal patterns by calculating the phase difference between epidemics at different locations. For cycles with a given period, the wavelet analysis generates a phase angle at each time step (Methods)[23]. This contrasts with standard multivariate spectral analysis, which can capture phase relationships at different periods[29], but does not allow a description of how they change with time. Because the raw phase spectrum is defined at each time step and period, it is difficult to interpret directly. We therefore focus on the phase of the relatively well defined (generally biennial) major epidemics, using wavelet reconstruction[23] (see Methods). We investigate the wavelet phases for periods between 1.5 and 3 years, using the wavelet reconstruction to calculate the average cycle and associated phase across these periods at each time step. This procedure allows naturally for observed spatio-temporal variations in major epidemic period and phase (Box 1).

The phase analysis is well illustrated by the pre-vaccination records for Norwich and Cambridge, because epidemics in these relatively close cities (90 km apart) were out of phase during the 1950s (ref. 30, Fig. 2). We also include results for London for comparison. The raw series (Fig. 2a) shows that major epidemics in Cambridge were aligned with London (and the national pattern) and occurred in odd years (1951, 1953, 1955, and so on). Norwich, by contrast, had epidemics that peaked in even years for the 15 years following World War Two. Figure 2c shows the major epidemic pattern for the three cities as revealed by the wavelet reconstruction. This confirms that the main epidemic period in London was predominantly biennial from around 1950; before that, epidemics tended to be more annual (Fig. 1a, b). More dramatically, the analysis highlights the early phase difference between Cambridge and Norwich (Fig. 2c–e), followed by the change in Norwich's epidemic phase from odd to even years in the late 1950s (we return below to the cause of Norwich's unusual even-year major epidemic timing). The analysis indicates that the biennial cycles of Cambridge and Norwich were 100 to 160° (7–11 months) out of phase for 16 years (Fig. 2e), after which they locked more closely into phase. Figure 2e also shows that major epidemics in Cambridge lagged several weeks behind those in London.

We observe from Fig. 2 that the phase difference between major epidemics changes relatively smoothly through time. This advances our objective of interpreting the complex spatio-temporal pattern of measles epidemics in terms of the spatial pattern of phase differences. For instance, phase-locked fluctuations (for example, refs 7 and 3) should result in zero phase-difference across the map, whereas travelling waves[1,4,5] should generate a phase difference that increases with distance.

We focus first on the 1950–66 period—after the 1947 baby boom but before vaccination—when the 2-year epidemic cycle was particularly pronounced (Fig. 1a). Figure 3a maps the average phase difference relative to London for the whole urban pre-vaccination data set (954 locations). Most, though not all, places lag behind London (88% have negative phase difference). Concentrating on the London region (Fig. 3c), there is a clear wave of infection moving away from the capital city. The wave is particularly well defined up to 30 km from London (Fig. 3c) with a wave speed of around 5 km per week. Figure 3d reveals the existence of a similar wave around Manchester. (We note that the focus of this wave is less well defined because there are several large cities—such as Leeds and Liverpool—that feed into the epidemic dynamics of North-western England.) The measles waves are illustrated dynamically in the Supplementary Information: the movie shows the raw incidence

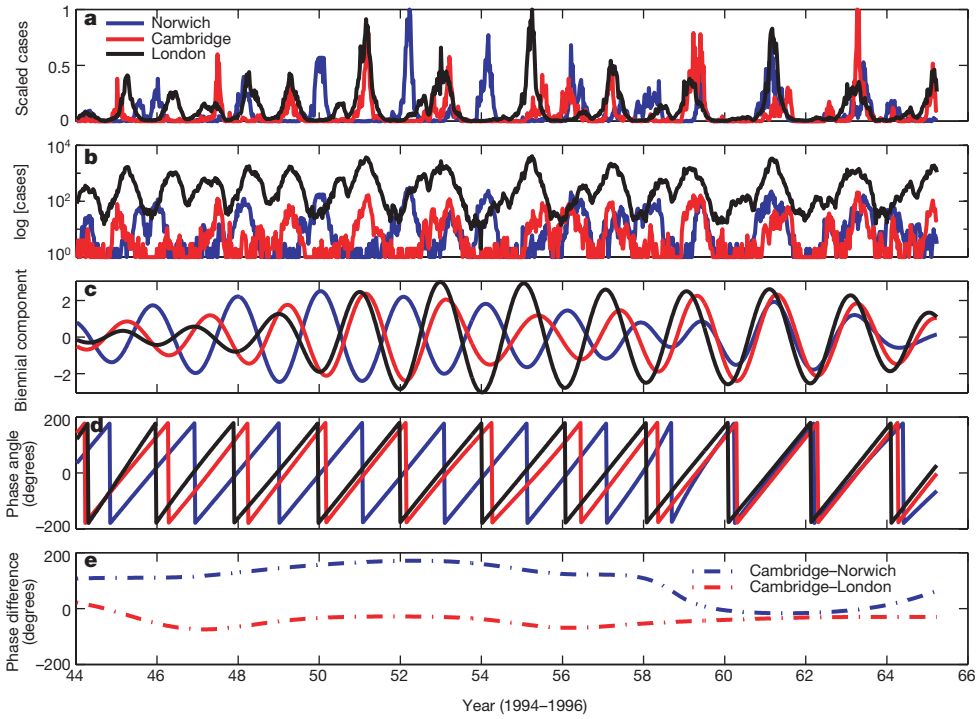

Figure 2 Wavelet phase analysis of weekly measles reports for Cambridge, Norwich and London in the pre-vaccine era. **a**, Pattern of weekly case reports. **b**, Logarithmic values of number of cases reported: $\log[x+1]$. **c**, Major epidemic (mainly biennial) component of the three series, reconstructed from wavelet spectral analysis (Box 1); the series were reconstructed from components in the period range 1.5 to 3 years, to allow for a flexible period ('multiannual' is probably therefore a better term than biennial, though the predominant variation is over 2 years). **d**, Average phase angles of the reconstructions in **c**. **e**, Phase difference between Cambridge and the other two cities, based on the phase angles in **d**; to remove spurious 'jumps in phase difference, the raw phase difference (θ) is constrained within $\pm 180°$, by the transformation: $\mathrm{mod}(\theta + 540, 360) - 180$, where $\mathrm{mod}(x, y)$ is x modulo y.

and phase analysis for the whole of England and Wales across seven epidemic cycles.

The time-averaged phase map (Fig. 3a) highlights the hierarchical nature of the waves, which move from large population centres to the surrounding hinterland throughout the 1950s and 60s. During this era, several hierarchical waves have their foci in large cities and spread progressively to more distant small towns (see also ref. 14). The dominant waves are those associated with London (Fig. 3c) and the northwestern industrial centre (Fig. 3d), but the hierarchical spread of infection is a consistent feature of the phase map, as is reflected in its spatial correlation structure (Fig. 4a, b; see below). An interesting feature of the pattern is that, although London—the biggest city—leads the epidemics in surrounding areas (Fig. 3a, c), the major epidemic appears on average 4–6 weeks before London in the urban northwest (Fig. 3a, d), moving from Liverpool and Manchester into the north Midlands. We speculate that this may arise from the unusual annual dynamics of Liverpool (which are due to high local birth rates[30]), effectively 'subsidizing' the growth of the epidemic in Manchester and Leeds and thereby sparking off early hierarchical waves in this region. Such regional heterogeneities are likely to be an interesting line of inquiry in future work. A second notable feature is the distinct pattern during the 1950s of even-year epidemics in the cities and villages of East Anglia, centred on Norwich (Fig. 3a, b). We speculate on the origin of this pattern in Box 2.

To quantify the geographic extent of the epidemic waves, we use spatial phase coherency functions (PCF)—calculated as the (non-parametric) spatial correlation function[7] of the major epidemic phases (Fig. 4a; see Methods). These functions express the correlation in phase angles at different locations as a function of intervening distance. During the pre-vaccination era, phases in nearby locations are generally found to be highly correlated. The correlation declines with distance to a distinct minimum at around 250 km, which possibly crudely reflects the spatial extent of the two dominant hierarchical waves. The PCF reveals that the local phase coherence was significantly higher than the regional average to a distance of around 100 km (Fig. 4a). In the vaccine era (Fig. 4a), the PCF resembles the pre-vaccination function in shape, but the average coherence is consistently and significantly lower. The extent of significant local phase coherence dropped to around 75 km during the 1970s. Extensions of the phase analysis (not shown) indicate that the hierarchical waves moving from large centres persist through the 1980s. However, the spatial extent of the waves dropped further (local coherence is only significant to 35 km), as high vaccination rates induced irregular epidemics later in the vaccine era[32].

Phase coherence effectively measures the relative timing of epidemics. A complementary approach is to consider the synchrony[7] of the epidemic time series (see Methods), which also reflects how their relative amplitudes covary. The pattern of synchrony in measles (Fig. 4b) follows the qualitative pattern of the phase coherency: declining with distance and with a lower mean in the vaccine era. However, the synchrony of epidemics is significantly less than their phase coherence, especially in the vaccine era. This indicates that vaccination induces stronger variations in the amplitude of epidemics than in their relative phase. Previous studies[32–34] have documented reductions in synchrony of measles epidemics as a result of vaccination. The present analysis reveals the detailed architecture of the change (Fig. 4b).

A 'forced forest fire' model for measles waves

The measles waves depart from the assumptions of classical theoretical models predicting travelling waves in two important ways. First, local transmission is strongly seasonally forced; second, the spatial distribution of the host is inherently very heterogeneous. We

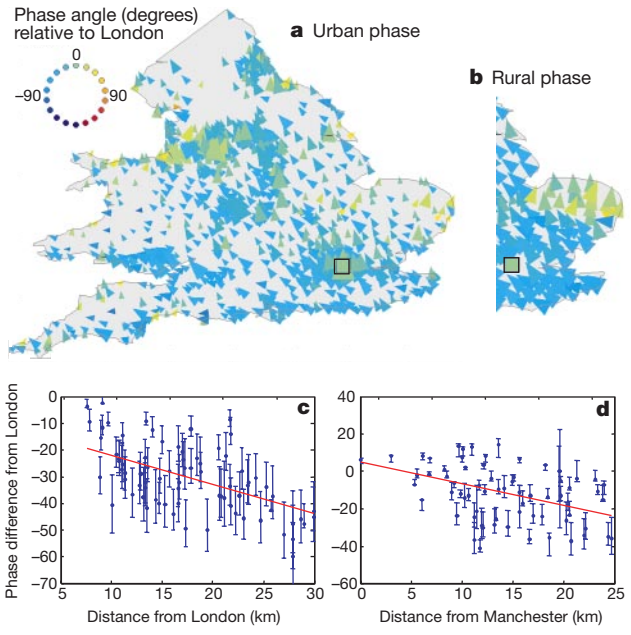

Figure 3 Phase differences from London for the full urban data set (954 locations). **a**, Urban mean phase differences from London for the pre-vaccination (1950–66) data, based on wavelet spectra (see Methods). Phases are coded by colour and angle as shown on the circular legend (see the Supplementary Information for more details). London is represented by a square. **b**, Phase differences from London of rural districts between London and Norwich; colour coding is as in **a**. **c**, Mean urban phase difference from London for 1950–66 in the London region, as a function of distance from the capital city. Within 30 km of London, there is a significant correlation of phase difference and distance ($r = -0.59$, 99% bootstrap limits: –0.75 to –0.39); the error bars are 99% bootstrapped confidence limits. **d**, As **c**, but showing phase difference from London in the Manchester area.

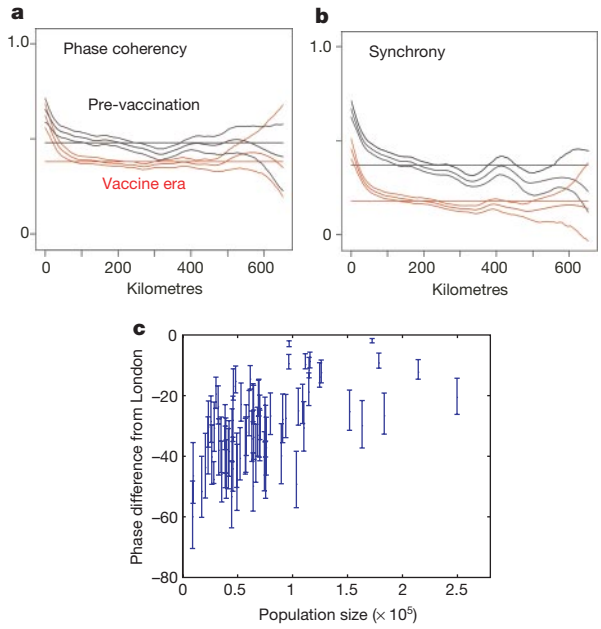

Figure 4 Pre-vaccination (black) and vaccine era (red). Spatial phase coherency function (**a**) and spatial synchrony of measles cases (**b**) with 95% confidence limits (see Methods). The horizontal bars represent the grand average phase coherence and grand average synchrony split into the pre-vaccination and vaccination eras. **c**, Phase difference from London as a function of population size for towns within 30 km of the capital (compare with Fig. 3c). Partial correlation analysis shows that phase difference is significantly and independently related both to distance from London ($r = -0.5$, $P < 0.001$; Fig. 3c) and population size ($r = 0.46$, $P < 0.0001$).

Box 2

Making waves

We investigated several different spatially coupled models for measles dynamics to understand the nature and cause of the hierarchical epidemic waves revealed by the wavelet analysis. Our most successful modelling framework to date builds on Bartlett's chain models[16], as refined in the time series SIR (TSIR) model[21,22,49]. The empirical waves are characterized by certain large cities (London and Manchester/Leeds) leading their local environs by a few to several weeks (Fig. 3c), with more complex relationships in more distant local areas. On the basis of the TSIR framework, we set up a simple coupled-map lattice, where at time $n+1$ the epidemic intensity, λ_{n+1}, is given as:

$$\lambda_{n+1} = \beta_n S_n (I_n + \theta_n)^{\alpha} \quad (1)$$

Here, β_n is a seasonal transmission rate, α is the mixing rate[21], S_n and I_n are respectively the number of local susceptible and infectious individuals in the previous characteristic time step (equal to 2 weeks, the approximate generation time for measles infection); θ_n is the (stochastic) contact rate with infectives, $\overline{I_n}$, in the neighbouring populations in the previous characteristic time step. We assume this rate to be Poisson distributed, θ_n is distributed as Po($m\overline{I_n}$), where m is the spatial coupling rate. According to the TSIR model, the epidemic birth-and-death process is realized according to a negative-binomial distribution[49] so that

$$I_{n+1} \text{ is distributed as NegBin}(\lambda_{n+1}, I_n) \quad (2)$$

The balance equation for the susceptibilities is $S_{n+1} = S_n + B - I_{n+1}$, where B is the birth rate. The parameter values closely match the best estimates for London and the estimated laws for how transmission scales with community size[49] (see Methods).

We envisage a human population distributed between a central city, composed of more tightly linked boroughs, and peripheral towns. Fig. 5a and b is generated from a linear map of a city with nine boroughs (shaded; for which m is arbitrarily set at 0.2) surrounded by the ten peripheral towns (for which m is set at 0.1):

In the above map, we assume that the population size is the same at all locations—this is not critical, but it makes interpretation easier. We contrast three situations.

In the first (Fig. 5a), each location is assumed to be below the CCS with 200,000 inhabitants. In an isolated town of this size, we would expect Type II dynamics[27]—regular biennial outbreaks, but with occasional local extinctions in the troughs. The dynamics from our spatial model show:

(1) High correlations between the tightly coupled boroughs (marked by black circles); the mean correlation is 0.79.

(2) Epidemics in the periphery lag behind those of the centre; the lag depends on the distance from the core (so that the mean correlations of the first through fifth periphery are 0.72, 0.63, 0.54, 0.50 and 0.45 respectively).

(3) The drop in correlation across the periphery is associated with a progressive time delay in peak incidence (by 1, 1.5, 2, 2.5 and 4 biweeks as we move from the nearest to the furthest peripheral town). This phase lag corresponds crudely to that seen in the data.

Figure 5a–c shows the mean of 10 biennia. Raw epidemic time series from the model give qualitatively similar results, as do the associated wavelet phases of the simulations (see the Supplementary Information). We stress that, whereas spatial coupling rates have been chosen somewhat arbitrarily and for illustrative purposes, all other parameters are estimated from data[49].

In the second case (Fig. 5b), each unit is above the CCS, with 3 million inhabitants. Consequently, each location exhibits persistent (Type I) biennial dynamics[27]. With local persistence at all locations, all are locked onto much more synchronized attractors than in Fig. 5a. The mean correlation between the boroughs is 0.98, and that between the boroughs and the periphery is 0.97. (A strictly deterministic model also generates similar results.) This relative phase locking contrasts markedly with the wave in Fig. 5a. See the Supplementary Information for a wavelet phase analysis of the model output.

Wave-like spatio-temporal behaviour might also result if there were a hierarchical trend of reduced infection rate as we move from large cities to smaller centres[15,50]. However, in practice, the basic reproductive ratio of measles infection, R_0, was relatively constant across the towns and cities of England and Wales[49], contradicting this alternative explanation. In fact, our simple coupling assumptions caused a slight increase in R_0 in the central city compared to the periphery, but its effect is small compared to the hierarchical invasion waves. The Supplementary Information explores these issues in more detail.

Finally, when we increase the arena of Fig. 5a to encompass a greater periphery (more small towns), we occasionally obtain travelling waves across the whole arena, as before. However, frequently we see a more complicated picture in which the more distant locations lock onto the other coexisting attractor (if the core peaked in even years, the periphery would peak in odd years, and *vice versa*). This is illustrated in Fig. 5c, where we use nine peripheral towns on either side of the city, rather than five. The simulation illustrates a very similar wave to Fig. 5a in the five inner towns of the periphery. By contrast, the outer four towns fall onto the opposite biennial attractor in this simulation. Such a reversal of phase can be stable for several epidemics and may give a qualitative explanation of the behaviour of Norwich and its environs (Fig. 1); isolation—and being near an edge (here the coast; see Supplementary Information)—increase the tendency for such jumps. Of course, towns are not connected only locally in terms of the movement of infection: an important area for future work is to consider how long-range 'jumps' of infection[6] obscure local waves and move the system closer to mean-field behaviour. We shall also consider how regional spatial structure interacts with population size and birth rate to influence the hierarchical pattern of waves.

focus on the relatively simple spatial hierarchy surrounding London in the pre-vaccination era (Figs 3c and 4c), in order to understand the essence of the epidemic waves. In this region, the wave moves fairly uniformly away from London (Fig. 3c). However, there is evidence that, in addition to distance, the local population size is important—smaller centres lag more than larger ones (Fig. 4c). Further analysis shows that both distance from London and population size contribute significantly to the epidemic lag (Fig. 4 legend).

This set of observations prompts the following conceptual model for the generation of travelling waves in childhood epidemics. Consider two epidemiologically coupled towns, with biennial measles cycles that are roughly in phase (for example, see Fig. 5a). Assume further that one town is large—above the critical community size (CCS) for measles persistence of around 300,000 (ref. 35)—and that the other town is below the CCS:

(1) After a large epidemic, susceptible densities build up to the deterministic threshold, above which another epidemic can happen[18].

(2) In the large town, measles is endemic throughout the inter-epidemic trough, so that a new epidemic occurs as soon as the effective reproductive ratio of infection exceeds unity[18]; this threshold is determined by the accumulation of susceptible children, modified by seasonally varying transmission rates associated with the school year.

(3) By contrast, in the small town, infection goes extinct locally after an epidemic; therefore, another epidemic cannot happen until an infective 'spark' is received, generally originating in a larger (endemic) community.

This reasoning prompts the following hypotheses:

(1) The spatial mosaic of large and small places is responsible for the lag in epidemics—we propose that having a group of small towns surrounding a large conurbation generates the hierarchical epidemic waves.

(2) As a corollary, coupling large centres (all above the CCS) should generate highly synchronized epidemics (as a result of nonlinear phase locking of seasonally forced oscillators)[31].

(3) Finally, weakly coupled or distant centres should have a stronger tendency than nearer towns to move onto the 'opposite' biennial attractor from the main conurbation.

We tested these conjectures using a mechanistic model for the spread of measles across a linear array of locally coupled sites (Box 2). The model generates a picture in tight agreement with our conceptual scenario. First, if we couple a central large city to an array of outlying towns below the CCS, we observe a spatio-temporal wave of infection. Epidemics in the outlying towns lag progressively behind those in the city (Fig. 5a). Note that dividing the city into tightly coupled 'boroughs' does not generate a lag within the large centre. Second, if we repeat the analysis by coupling a series of large communities all above the CCS, the result is near-perfect coherence, with no evidence of epidemic waves (Fig. 5b). Because epidemics do not suffer local extinction, and because all the cities experience the same seasonal forcing, no lags are generated. Thus, the observed travelling waves are best seen as repeated and very fast invasion waves, extending from endemic core areas into epidemic satellite regions.

Third, we examine the effects of relative epidemiological isolation by extending the array of distant, more loosely coupled communities (Fig. 5c). As before, synchronized major epidemics with superimposed spatio-temporal waves appear for small communities close to the large one. However, epidemics in more distant towns can drop onto the opposite biennial attractor. This is preliminary evidence that relative isolation may be a source of the unusual 'even year' behaviour of pre-vaccination measles epidemics in Norwich and its environs (Fig. 2), during parts of the pre-vaccination era.

Our study raises a number of issues. We illustrate how wavelets can be used for analysing both non-stationary time series and spatio-temporal patterns in ecology and population biology. Spatial and temporal non-stationarity is the norm in ecology. It may be caused by a number of factors, including anthropogenic influences and biological evolution, as well as more esoteric dynamical effects, such as coexisting attractors[20,36] and intermittent periodicity in chaos[37]. Wavelets are emerging as essential tools in the study of intermittent processes in the physical sciences and experimental biology[26]. Here we have illustrated a basic application of wavelet analysis in population dynamics, complementing previous applications to spatial transect patterns[38]; there should be significant scope for further careful ecological application of wavelets. The wavelet phase analysis also provides an unusual method for analysing ecological travelling waves. Although other statistical models have been successfully developed[11,39], wavelet phase angles are naturally suited to allowing for variations in cycle period and amplitude.

In addition, the non-stationarity that we demonstrate in the measles series is due mainly to variations in the recruitment of susceptible individuals, driven by birth rates and especially by the onset of vaccination[22,32]. Mass immunization caused a dramatic fall in susceptible recruitment rates and a marked reduction in the spatial correlation and coherence of epidemics: this may have important consequences for the design of vaccination programmes[19,32]. The implications of hierarchical ('core–satellite') epidemic dynamics for the control of established and emergent diseases are important areas for future research.

Finally, our analysis demonstrates prominent repeated spatio-temporal waves, superimposed on the well-known epidemic time series of measles in England and Wales. This echoes, on a more extensive spatio-temporal scale, seminal work on the hierarchical spatial diffusion of measles epidemics[14]. The simplicity of the measles dynamical 'clockwork' and the intricacy of the human demographic record allow us this unusual opportunity to quantify the impact of spatio-temporal heterogeneities on epidemic dynamics. The clearest temporal transition is the effect of mass vaccination. On a shorter timescale, seasonal variation in infection rate is a major driver of the dynamics[40,41]. Classical reaction–diffusion models of host–natural enemy systems often predict recurring travelling waves in homogeneous (non-hierarchical) systems[1]. However, such waves are precluded for measles, because of the strongly synchronizing effect of seasonally forced transmission[31]. Previous theory[31,33,42] indicates that seasonally driven epidemics will either be completely synchronized across large coupled centres or more irregular in small centres buffeted by demographic noise.

This prediction is at odds with the observed waves (Figs 3 and 4),

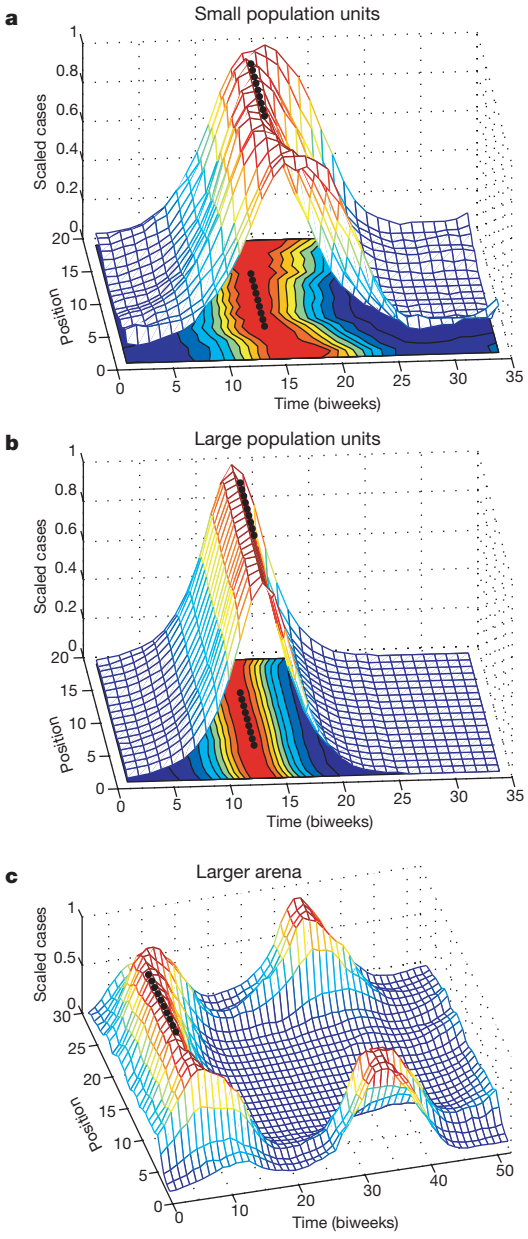

Figure 5 Average biennial behaviour of a spatially coupled measles model (see Box 2 for details). **a**, Coupling relatively small peripheral population units (below the critical community size, CCS, for measles persistence) to a central 'city'. **b**, Coupling larger populations (each above the CCS) to the city. **c**, As in **a**, but extending the size of the linear array of populations.

leading us to propose a different underlying mechanism—measles waves arise as repeated invasions from endemic core areas to the periphery. The coupling of large and small centres may thus be the critical feature that generates waves in these seasonally forced systems. This mechanism has analogies with the operation of the 'rescue effect' in core–satellite metapopulations[43] and also with forest fire dynamics[44]. Forest-fire-like epidemic dynamics have previously been explored in the irregular, epidemic measles outbreaks observed on isolated small islands[45]. This work provides evidence of such phenomena in an endemic epidemiological context. □

Methods

The data

We use weekly official measles notifications and associated demographic data for England and Wales[15,19,46]. For the pre-vaccination era, before 1966, weekly measles case data are available for 945 cities and towns and 457 rural districts; these data sets are the basis of the pre-vaccination wavelet analysis (Figs 2, 3a, b and 4c). In 1974, boundary changes agglomerated the spatial data into 354 administrative areas. To achieve consistent time series across both pre-vaccination and vaccine era, we have therefore binned the pre-vaccination data into the post-1974 boundaries (Figs 1 and 4a, b).

Wavelet time series analysis

See Box 1. All series are logarithm transformed (after adding a constant of one) to make them more sinusoidal, and subsequently scaled to zero mean and unit variance. Assume that we have a time series, I_n, $n = 0, \ldots, T-1$ (for consistency, n is used as the time index throughout the paper). We analyse temporal changes in the distribution of power at different scales s (approximately periods) using a Morlet wavelet function, $\psi_0(\eta) = \pi^{-1/4} \exp(i\omega_0\eta) \exp(-\eta^2/2)$, where ω_0 is the non-dimensional frequency here taken to be 6 (ref. 23) and $\eta = n/s$. The Morlet wavelet, ψ_0, is a damped complex exponential (Box 1).

The continuous wavelet transform (CWT), $W_n(s)$, of the time series $I_n(n = 0, 1, 2\ldots)$ is calculated as the convolution of I_n with a scaled and translated version of ψ_0 (ref. 23). For the Morlet wavelet, scale is approximately equal to the Fourier period, so that the lowest scale, s_0, roughly corresponds to the maximum (Nyquist) frequency of 0.5 cycles per time step. The local wavelet power spectrum (Box 1), at time point n and scale s is then given by $|W_n(s)|^2$.

To minimize biases due to edge effects, the data were padded with zeros, up to the next-highest power of two[23]. The 'cone of influence' (the parabola in Fig. 1b) is a reflection of a consequent loss in statistical power near the start and end of the series; the area below the parabola in Fig. 1b should be interpreted cautiously. The width of the cone also gives a rough lower limit for how wide a feature needs to be at a given scale for it to represent genuine cyclical behaviour, rather than a spike. We conduct significance tests using methods described and discussed in ref. 23.

To isolate the major biennial epidemics for the phase analysis, we use wavelet reconstruction[23] to partition the original series, in terms of the contribution of variation at different frequencies.

Phase relationships between time series

A wavelet transform based on a complex wavelet, such as the Morlet wavelet, has a phase angle, defined by

$$\Theta_n(s) = \arctan\{\mathrm{Im}[W_n(s)]/\mathrm{Re}[W_n(s)]\}$$

where $\mathrm{Re}[W_n(s)]$ is the real, and $\mathrm{Im}[W_n(s)]$ the imaginary part of $W_n(s)$. In practice, we use this formula to calculate the time series of phase angles (θ_n) associated with the wavelet transform of the reconstructed major epidemic cycle for each time series. These can be used as absolute phases (Fig. 2d) or phase differences (Fig. 2e); phases and phase differences are restricted to the range $\pm 180°$ (see Fig. 2, legend).

Algorithms

The algorithms and notation used here are based on a practical guide to meteorological wavelet analysis[23]. See also http://paos.colorado.edu/research/wavelets/ for more background information. The website also includes a set of wavelet algorithms in Matlab, on which the analyses shown here are based.

Phase coherency and correlation functions

We calculate the phase coherency, $\vartheta_{i,j}$, between two cities, i and j, by considering the correlation between the time series of phase angles, $\theta_{i,n}$ and $\theta_{j,n}$:

$$\vartheta_{ij} = \sum_n (\theta_{i,n} - \bar{\theta}_i)(\theta_{j,n} - \bar{\theta}_j)/\sigma_i\sigma_j$$

where $\bar{\theta}$ represents the respective mean phases, and σ the respective standard deviation of the phases. We further define the phase coherency function, $\eta(d)$, which governs how the phase coherency relates to the distance, d, separating any two cities. Assuming that the phase coherency forms a stationary random field, then the phase coherency function (PCF) represents the spatial correlation function of that field. We estimate the PCF, without making *a priori* assumptions about the functional form, by using the nonparametric covariance function (NCF)[7,47,48]. The NCF uses either a kernel function or (as in our case) a cubic B-spline to estimate the underlying correlation function. We use a smoothing spline with 25 equivalent degrees of freedom (e.d.f.), and quantify the confidence envelopes for the functions using 500 bootstrap iterations (see ref. 48 for details of estimation and testing).

We measure epidemic synchrony between two populations as the Pearson correlation coefficient between the two variance-stabilized (square-root transformed) time series of incidence. We calculate the spatial correlation functions governing how this synchrony depends on distance—again, using the nonparametric spline covariance function. Separate phase coherency and spatial correlation functions are calculated for the pre-vaccination (1954–64) and vaccination (1970–80) data, based on the 354 time series that span both eras.

The spatial TSIR model

We used the following parameters for the model in Box 2: $\alpha = 0.97$, and $\{\beta_n\}$ is an annually periodic function with the following values for the 26 biweeks of the year: 1.11×10^{-5}, 1.11×10^{-5}, 1.10×10^{-5}, 1.09×10^{-5}, 1.06×10^{-5}, 1.03×10^{-5}, 1.01×10^{-5}, 9.84×10^{-6}, 9.63×10^{-6}, 9.40×10^{-6}, 9.10×10^{-6}, 8.71×10^{-6}, 8.29×10^{-6}, 7.89×10^{-6}, 7.60×10^{-6}, 7.49×10^{-6}, 7.60×10^{-6}, 7.93×10^{-6}, 8.42×10^{-6}, 8.95×10^{-6}, 9.43×10^{-6}, 9.80×10^{-6}, 1.01×10^{-5}, 1.03×10^{-5}, 1.05×10^{-5}, 1.08×10^{-5}. These values are a smoothed version of the estimated parameters for the London time series[49]. The biweekly birth rate, B, is set at 100 for small population units (Fig. 5a) and 2,000 for large ones (Fig. 5b).

Received 4 May; accepted 12 October 2001.

1, Murray, J. D. *Mathematical Biology* (Springer, London, 1989).
2. Neubert, M. G., Kot, M. & Lewis, M. A. Dispersal and pattern formation in a discrete-time predator–prey model. *Theor. Pop. Biol.* **48,** 7–43 (1995).
3. Sherratt, J. A. Periodic travelling waves in cyclic predator–prey systems. *Ecol. Lett.* **4,** 30–37 (2001).
4. Hassell, M. P., Comins, H. N. & May, R. M. Spatial structure and chaos in insect population dynamics. *Nature* **353,** 255–258 (1991).
5. Sole, R. V., Valls, J. & Bascompte, J. Spiral waves, chaos and multiple attractors in lattice models of interacting populations. *Phys. Lett. A* **166,** 123–128 (1992).
6. Jeltsch, F., Muller, M. S., Grimm, V., Wissel, C. & Brandl, R. Pattern formation triggered by rare events: Lessons from the spread of rabies. *Proc. R. Soc. Lond. B* **264,** 495–503 (1997).
7. Bjørnstad, O. N., Ims, R. A. & Lambin, X. Spatial population dynamics: analysing patterns and processes of population synchrony. *Trends Ecol. Evol.* **14,** 427–432 (1999).
8. Blasius, B., Huppert, A. & Stone, L. Complex dynamics and phase synchronization in spatially extended ecological systems. *Nature* **399,** 354–359 (1999).
9. Mollison, D. Modeling biological invasions—chance, explanation, prediction. *Phil. Trans. R. Soc. Lond. B* **314,** 675–693 (1986).
10. Bulmer, M. G. A statistical analysis of the 10-year cycle in Canada. *J. Anim. Ecol.* **43,** 701–718 (1974).
11. Lambin, X., Elston, D. A., Petty, S. J. & MacKinnon, J. L. Spatial asynchrony and periodic travelling waves in cyclic populations of field voles. *Proc. R. Soc. Lond. B* **265,** 1491–1496 (1998).
12. Ranta, E. & Kaitala, V. Travelling waves in vole population dynamics. *Nature* **390,** 456–456 (1997).
13. Stenseth, N. C. *et al.* Common dynamic structure of Canada lynx populations within three climatic regions. *Science* **285,** 1071–1073 (1999).
14. Cliff, A. D., Haggett, P. & Smallman-Raynor, M. *Measles: An Historical Geography of a Major Human Viral Disease from Global Expansion to Local Retreat, 1840–1990* (Blackwell, Oxford, 1993).
15. Grenfell, B. T. & Bolker, B. M. Cities and villages: infection hierarchies in a measles metapopulation. *Ecol. Lett.* **1,** 63–70 (1998).
16. Bartlett, M. S. in *Proc. Third Berkeley Symp. on Mathematical Statistics and Probability* Vol. 4, 81–109 (Univ. California Press, Berkeley, 1956).
17. Schenzle, D. An age-structured model of pre- and post-vaccination measles transmission. *IMA J. Math. Appl. Med. Biol.* **1,** 169–191 (1984).
18. Anderson, R. M. & May, R. M. *Infectious Diseases of Humans: Dynamics and Control* (Oxford Univ. Press, Oxford, 1991).
19. Grenfell, B. T. & Harwood, J. (Meta)population dynamics of infectious diseases. *Trends Ecol. Evol.* **12,** 395–399 (1997).
20. Earn, D. J. D., Rohani, P., Bolker, B. M. & Grenfell, B. T. A simple model for complex dynamical transitions in epidemics. *Science* **287,** 667–670 (2000).
21. Finkenstädt, B. F. & Grenfell, B. T. Time series modelling of childhood diseases: a dynamical systems approach. *J. R. Stat. Soc. C* **49,** 187–205 (2000).
22. Grenfell, B. T., Bjornstad, O. N. & Finkenstädt, B. F. Dynamics of measles epidemics. II. Scaling noise, determinism and predictability with the time series SIR model. *Ecol. Monogr.* (in the press).
23. Torrence, C. & Compo, G. P. A practical guide to wavelet analysis. *Bull. Am. Meteorol. Soc.* **79,** 61–78 (1998).
24. Nason, G. P. & von Sachs, R. Wavelets in time series analysis. *Phil. Trans. R. Soc. Lond. A* **357,** 2511–2526 (1999).
25. Daubechies, I. *Ten Lectures on Wavelets* (Society for Industrial and Applied Mathematics, Philadelphia, 1992).
26. Percival, D. B. & Walden, A. T. *Wavelet Methods for Time Series Analysis* (Cambridge Univ. Press, Cambridge, 2000).
27. Bartlett, M. S. Measles periodicity and community size. *J. R. Stat. Soc. A* **120,** 48–70 (1957).
28. Anderson, R. M., Grenfell, B. T. & May, R. M. Oscillatory fluctuations in the incidence of infectious disease and the impact of vaccination: time series analysis. *J. Hyg.* **93,** 587–608 (1984).
29. Chatfield, C. *The Analysis of Time Series: An Introduction* (Chapman and Hall, London, 1996).
30. Finkenstädt, B. F. & Grenfell, B. T. Empirical determinants of measles metapopulation dynamics in England and Wales. *Proc. R. Soc. Lond. B* **265,** 211–220 (1998).
31. Lloyd, A. L. & May, R. M. Spatial heterogeneity in epidemic models. *J. Theor. Biol.* **179,** 1–11 (1996).
32. Earn, D., Rohani, P. & Grenfell, B. T. Spatial dynamics and persistence in ecology and epidemiology. *Proc. R. Soc. Lond. B* **265,** 7–10 (1998).

33. Bolker, B. M. & Grenfell, B. T. Impact of vaccination on the spatial correlation and dynamics of measles epidemics. *Proc. Natl Acad. Sci. USA* **93,** 12648–12653 (1996).
34. Cliff, A. D., Haggett, P., Stroup, D. F. & Cheney, E. The changing geographical coherence of measles morbidity in the United States, 1962–88. *Stat. Med.* **11,** 1409–1424 (1992).
35. Bartless, M. S. The critical community size for measles in the U.S. *J. R. Stat. Soc. A* **123,** 37–44 (1960).
36. Grenfell, B. T., Bolker, B. M. & Kleczkowski, A. Seasonality and extinction in chaotic metapopulations. *Proc. R. Soc. Lond. B* **259,** 97–103 (1995).
37. Kendall, B. E., Schaffer, W. M. & Tidd, C. W. Transient periodicity in chaos. *Phys. Lett. A* **177,** 13–20 (1993).
38. Bradshaw, G. A. & Spies, T. A. Characterizing canopy gap structure in forests using wavelet analysis. *J. Ecol.* **80,** 205–215 (1992).
39. Bjørnstad, O. N. & Bascompte, J. Synchrony and second order spatial correlation in host-parasitoid systems. *J. Anim. Ecol.* **70,** 924–933 (2001).
40. Schaffer, W. M. & Kot, M. Nearly one dimensional dynamics in an epidemic. *J. Theor. Biol.* **112,** 403–427 (1985).
41. Schwartz, I. B. in *Biomedical Modelling and Simulation* (eds Eisenfeld, J. & Levine, D. S.) 201–204 (Scientific, New York, 1989).
42. Bolker, B. M. & Grenfell, B. T. Space, persistence and the dynamics of measles epidemics. *Phil. Trans. R. Soc. Lond. B* **348,** 309–320 (1995).
43. Hanski, I. & Gyllenberg, M. Two general metapopulation models and the core-satellite hypothesis. *Am. Nat.* **142,** 17–41 (1993).
44. Bak, P. *How Nature Works—The Science of Organised Criticality* (Oxford Univ. Press, Oxford, 1977).
45. Rhodes, C. J. & Anderson, R. M. Power laws governing epidemics in isolated populations. *Nature* **381,** 600–602 (1996).
46. Office of Population Censuses and Surveys *Registrar General's Weekly Return for England and Wales* (Her Majesty's Stationery Office (HMSO), London, 1944–94).
47. Hall, P. & Patil, P. Properties of nonparametric estimators of autocovariance for stationary random fields. *Prob. Theor. Relat. Fields* **99,** 399–424 (1994).
48. Bjørnstad, O. N. & Falck, W. Nonparametric spatial covariance functions: estimation and testing. *Environ. Ecol. Stat.* **8,** 53–70 (2001).
49. Bjørnstad, O. N., Finkenstädt, B. & Grenfell, B. T. Dynamics of measles epidemics. I. Estimating scaling of transmission rates using a time series SIR model. *Ecol. Monogr.* (in the press).
50. May, R. M. & Anderson, R. M. Spatial heterogeneity and the design of immunization programs. *Math. Biosci.* **72,** 83–111 (1984).

Supplementary Information accompanies the paper on *Nature*'s website (http://www.nature.com).

Acknowledgements

We thank S. Cornell, T. Coulson, J. Gog, M. Keeling, A. Lloyd, G. Nason, P. Rohani, C. Torrence and C. Williams for helpful discussions. B.T.G. and J.K. were supported by the Wellcome Trust. O.N.B. was supported by the National Center for Ecological Analysis and Synthesis (a Centre funded by an NSF grant, the University of California Santa Barbara, and the State of California) and the Norwegian Science Foundation.

Correspondence and requests for materials should be addressed to B.T.G. (e-mail: b.t.grenfell@zoo.cam.ac.uk).